

Fast optimal entrainment of limit-cycle oscillators by strong periodic inputs via phase-amplitude reduction and Floquet theory

Shohei Takata,^{1, a)} Yuzuru Kato,^{1, b)} and Hiroya Nakao^{1, c)}

*Department of Systems and Control Engineering, Tokyo Institute of Technology,
Tokyo 152-8552, Japan*

(Dated: 18 August 2022)

Optimal entrainment of limit-cycle oscillators by strong periodic inputs is studied on the basis of the phase-amplitude reduction and Floquet theory. Two methods for deriving the input waveforms that keep the system state close to the original limit cycle are proposed, which enable the use of strong inputs for entrainment. The first amplitude-feedback method uses feedback control to suppress deviations of the system state from the limit cycle, while the second amplitude-penalty method seeks an input waveform that does not excite large deviations from the limit cycle in the feedforward framework. Optimal entrainment of the Van der Pol and Willamowski-Rössler oscillators with real or complex Floquet exponents are analyzed as examples. It is demonstrated that the proposed methods can achieve much faster entrainment and provide wider entrainment ranges than the conventional method that relies only on phase reduction.

^{a)}E-mail: takata.s.ae@m.titech.ac.jp

^{b)}Corresponding author. E-mail: kato.y.bg@m.titech.ac.jp

^{c)}E-mail: nakao@sc.e.titech.ac.jp

Entrainment of self-sustained oscillators by periodic inputs is widely observed in the real world, including the entrainment of circadian rhythms to sunlight and injection locking of electrical oscillators to clock signals. Optimization of input waveforms for stable entrainment has been considered by using phase reduction, which often neglects amplitude deviations of the oscillator state from the original orbit. However, such methods do not perform well for strong inputs because the phase-only approximation breaks down. In this study, using phase-amplitude reduction, we propose two methods for obtaining input waveforms that can suppress amplitude deviations. We demonstrate that both methods enable us to apply stronger periodic inputs and achieve faster entrainment.

I. INTRODUCTION

Synchronization or entrainment is a phenomenon in which rhythms of self-sustained oscillators adjust with each other or adjust to periodic external inputs. It is observed in a variety of real-world systems including metronomes¹, Belousov-Zhabotinsky chemical reaction², flashing fireflies³⁻⁵, circadian rhythms^{6,7}, and many others⁸⁻¹³. Entrainment of nonlinear limit-cycle oscillators by external periodic inputs, also known as injection locking, finds many technological applications such as the frequency tuning in millimeter-wave oscillators^{14,15}, frequency stabilization of class-E electrical oscillators¹⁶, suppression of pulsus alternans in the heart^{17,18}, and adjustment of circadian rhythms^{7,19}.

When the input given to the limit-cycle oscillator is sufficiently weak, the phase reduction theory can be used to analyze the oscillator dynamics^{8-10,20-22}, which allows us to describe multidimensional nonlinear dynamics of the oscillator by an approximate one-dimensional phase equation. It has been extensively used in the analysis of coupled oscillators¹¹, in particular, in explaining their collective synchronized dynamics^{9,23,24}. Recently, the phase reduction theory has been formulated also for non-conventional physical systems, such as piecewise-smooth oscillators²⁵, oscillators with time delay²⁶, rhythmic spatiotemporal patterns^{27,28}, and quantum limit-cycle oscillators²⁹.

The phase equation can also be used to formulate optimization and control problems

for limit-cycle oscillators²¹, for example, minimizing the control power^{30–33}, maximizing the locking range^{34–36} and linear stability³⁷ in the entrainment, maximizing the linear stability of mutual synchronization between coupled oscillators^{38,39}, maximizing the phase coherence of noisy oscillators⁴⁰, performing phase-selective entrainment of oscillators⁴¹, and controlling the phase distributions in oscillator populations^{42–45}. Optimization methods based on phase reduction have also been studied in non-conventional oscillatory systems such as mutual synchronization between rhythmic spatiotemporal patterns⁴⁶ and collectively oscillating networks⁴⁷, and entrainment of a quantum limit-cycle oscillator in the semiclassical regime⁴⁸. However, these methods do not perform well when the driving input given to the oscillator is not sufficiently weak because the amplitude deviations of the system state from the unperturbed limit cycle become non-negligible and the phase-only description of the system state breaks down; this is a fundamental limitation hampering practical applications of all methods that rely only on phase reduction.

Recent developments in the Koopman operator theory^{49,50} have clarified that the deviations of the system state from the limit cycle can be characterized naturally by the amplitude variables, which are Koopman eigenfunctions associated with non-zero Floquet exponents of the system⁵¹. Phase-amplitude reduction theories that generalize the conventional phase-only reduction theory by including the amplitude variables have also been formulated^{21,52–57}. By using the resulting phase-amplitude equations, optimization methods have been proposed^{18,55,58,59}, for example, for minimizing the control power applied to the oscillator with slow amplitude relaxation.

In this study, on the basis of the phase-amplitude reduction and Floquet theory, we propose two methods to realize fast entrainment of the oscillator by applying strong inputs: an *amplitude-feedback method*, which applies feedback control in addition to the optimal input for phase locking, and an *amplitude-penalty method*, which is in the feedforward framework and gives the optimal input that does not excite amplitude deviations. Using the Van der Pol and Willamowski-Rössler oscillators as examples, we demonstrate that the proposed methods can significantly improve the convergence time to the entrained state and enlarge the entrainment range.

This paper is organized as follows; in Sec. 2, the phase-amplitude reduction and Floquet theory are briefly explained; in Sec. 3, the conventional optimization method for stable entrainment based on phase-only reduction is reviewed and its failure for strong inputs

is demonstrated; in Sec. 4, the amplitude-feedback and amplitude-penalty methods are proposed on the basis of phase-amplitude reduction; in Sec. 5, the validity of the proposed methods are demonstrated by using the Van der Pol and Willamowski-Rössler oscillators; in Sec. 6, conclusions and discussion are given, and in the Appendix, additional discussions on the optimal tangential input and details of the numerical methods for calculating the Floquet eigenvectors are given.

II. PHASE-AMPLITUDE REDUCTION AND FLOQUET THEORY

In this section, we briefly review the phase-amplitude reduction theory for limit-cycle oscillators and its relation to the Floquet theory.

A. Phase-amplitude reduction

We begin with a brief introduction of the phase-amplitude reduction^{52–55}. We consider a limit-cycle oscillator described by

$$\dot{\mathbf{X}}(t) = \mathbf{F}(\mathbf{X}(t)), \quad (1)$$

where $\mathbf{X}(t) \in \mathbb{R}^N$ is the system state at time t , the overdot ($\dot{}$) denotes the time derivative, and $\mathbf{F}(\mathbf{X}) \in \mathbb{R}^N$ describes the oscillator dynamics. It is assumed that Eq. (1) has an exponentially stable limit-cycle solution $\mathbf{X}_0(t) = \mathbf{X}_0(t + T)$ with period $T = 2\pi/\omega$, where ω is the natural frequency. We denote this limit cycle as χ .

The linear stability of χ is characterized by the Floquet exponents λ_i ($i = 0, 1, \dots, N-1$). One of the exponents vanishes, $\lambda_0 = 0$, which is associated with the phase direction tangent to χ , and the other exponents $\lambda_1, \dots, \lambda_{N-1}$ associated with the amplitude deviations from χ possess negative real parts and are in general complex. These Floquet exponents are sorted in decreasing order of their real parts, i.e., $\lambda_0 = 0 > \text{Re}(\lambda_1) \geq \text{Re}(\lambda_2) \geq \dots \geq \text{Re}(\lambda_{N-1})$.

For this system, we can define a phase function $\Theta(\mathbf{X}) : \mathbb{R}^N \rightarrow [0, 2\pi)$ and amplitude functions $R_i(\mathbf{X}) : \mathbb{R}^N \rightarrow \mathbb{C}$ ($i = 1, \dots, N-1$) in the basin of χ satisfying

$$\begin{aligned} \dot{\Theta}(\mathbf{X}) &= \langle \nabla \Theta(\mathbf{X}), \mathbf{F}(\mathbf{X}) \rangle = \omega, \\ \dot{R}_i(\mathbf{X}) &= \langle \nabla R_i(\mathbf{X}), \mathbf{F}(\mathbf{X}) \rangle = \lambda_i R_i(\mathbf{X}), \end{aligned} \quad (2)$$

where the inner product is defined by $\langle \mathbf{a}, \mathbf{b} \rangle = \sum_{j=1}^N a_j^* b_j$ (* denotes complex conjugate). It is noted that the phase constantly increases with the frequency ω and the amplitudes decay linearly with the rate (possibly complex) λ_i , namely, the phase and amplitude functions provide a global linearization of the original nonlinear system in the basin of χ ⁵¹.

Using the phase and amplitude functions Θ and R_i , we introduce the phase and amplitude variables of the system state \mathbf{X} as $\theta = \Theta(\mathbf{X})$ and $r_i = R_i(\mathbf{X})$ ($i = 1, \dots, N-1$). When the state $\mathbf{X}(t)$ is on χ , it can be represented as a function of the phase as $\mathbf{X}(t) = \mathbf{X}_0(\theta/\omega) =: \chi(\theta)$, where the state $\mathbf{X}_0(0)$ at $t = 0$ is chosen as the origin $\theta = 0$ of the phase without loss of generality, and the symbol $\chi(\theta)$ is introduced to represent the state on the limit cycle χ as a function of the phase θ . Each amplitude $R_i(\mathbf{X})$ measures the deviation of the system state \mathbf{X} from χ and vanishes when \mathbf{X} is on χ , i.e., $R_i(\chi(\theta)) = 0$.

The phase defined above is called the *asymptotic phase*^{8-11,20} and characterizes the oscillator dynamics along χ . The level sets of this phase function is called *isochrons*. Similarly, the level sets of the (absolute values of the) amplitudes characterizing deviations of the system state from χ are called *isostables*⁵¹. The exponential of the phase function $e^{\sqrt{-1}\Theta(\mathbf{X})}$ and the amplitude functions $R_i(\mathbf{X})$ are Koopman eigenfunctions of Eq. (1), satisfying $\langle \mathbf{F}(\mathbf{X}), \nabla e^{\sqrt{-1}\Theta(\mathbf{X})} \rangle = \sqrt{-1}\omega e^{\sqrt{-1}\Theta(\mathbf{X})}$ and $\langle \mathbf{F}(\mathbf{X}), \nabla R_i(\mathbf{X}) \rangle = \lambda_i R_i(\mathbf{X})$, respectively^{22,51}.

We now assume that the oscillator is perturbed as

$$\dot{\mathbf{X}}(t) = \mathbf{F}(\mathbf{X}(t)) + \mathbf{p}(\mathbf{X}(t), t), \quad (3)$$

where the perturbation $\mathbf{p}(\mathbf{X}, t) \in \mathbb{R}^N$ can depend on \mathbf{X} and t . By using the chain rule of differentiation, we can derive the equations for the phase and amplitudes variables as

$$\begin{aligned} \dot{\theta}(t) &= \omega + \langle \nabla \Theta(\mathbf{X}(t)), \mathbf{p}(\mathbf{X}(t), t) \rangle, \\ \dot{r}_i(t) &= \lambda_i r_i(t) + \langle \nabla R_i(\mathbf{X}(t)), \mathbf{p}(\mathbf{X}(t), t) \rangle. \end{aligned} \quad (4)$$

If we can express \mathbf{X} as a function of θ and r_1, \dots, r_{N-1} , we obtain a closed set of phase-amplitude equations. However, in general, we are interested in the phase θ and only a small number of slowly decaying amplitudes r_1, \dots, r_M ($M < N-1$) to reduce the dimensionality of the system. In this case, we cannot uniquely express \mathbf{X} as a function of θ and r_1, \dots, r_M and we need to introduce some approximation to obtain a reduced set of phase-amplitude equations with smaller dimensionality.

In the conventional phase reduction for a weakly perturbed limit-cycle oscillator^{9,20}, it is assumed that the perturbation \mathbf{p} is sufficiently weak and of order $\mathcal{O}(\epsilon)$ where $0 \leq \epsilon \ll 1$. We denote the perturbation as $\mathbf{p} = \epsilon \mathbf{P}$ where \mathbf{P} is of order $\mathcal{O}(1)$. Since the system state \mathbf{X} is close to χ in this case, we can approximate it as $\mathbf{X} = \chi(\theta) + \mathcal{O}(\epsilon)$ where $\theta = \Theta(\mathbf{X})$. It then follows that $\nabla\Theta(\mathbf{X}) = \nabla\Theta(\mathbf{X})|_{\mathbf{X}=\chi(\theta)} + \mathcal{O}(\epsilon)$, $\nabla R_i(\mathbf{X}) = \nabla R_i(\mathbf{X})|_{\mathbf{X}=\chi(\theta)} + \mathcal{O}(\epsilon)$, and $\mathbf{P}(\mathbf{X}, t) = \mathbf{P}(\chi(\theta), t) + \mathcal{O}(\epsilon)$. Plugging these expressions into Eq. (4), we obtain

$$\begin{aligned}\dot{\theta} &= \omega + \epsilon \langle \mathbf{Z}(\theta), \mathbf{P}(\chi(\theta), t) \rangle + \mathcal{O}(\epsilon^2), \\ \dot{r}_i &= \lambda_i r_i + \epsilon \langle \mathbf{I}_i(\theta), \mathbf{P}(\chi(\theta), t) \rangle + \mathcal{O}(\epsilon^2).\end{aligned}\tag{5}$$

Here, we introduced the phase sensitivity function (PSF) $\mathbf{Z}(\theta) = \nabla\Theta|_{\mathbf{X}=\chi(\theta)}$ and amplitude (isostable) sensitivity functions (ISFs) $\mathbf{I}_i(\theta) = \nabla R_i|_{\mathbf{X}=\chi(\theta)}$, which are the gradients of the phase and amplitude functions evaluated at $\mathbf{X} = \chi(\theta)$ on χ . Neglecting the terms of order $\mathcal{O}(\epsilon^2)$ and using the original notation \mathbf{p} for the perturbation, we obtain the approximate phase-amplitude equations at the lowest order,

$$\begin{aligned}\dot{\theta} &= \omega + \langle \mathbf{Z}(\theta), \mathbf{p}(\chi(\theta), t) \rangle, \\ \dot{r}_i &= \lambda_i r_i + \langle \mathbf{I}_i(\theta), \mathbf{p}(\chi(\theta), t) \rangle.\end{aligned}\tag{6}$$

In this study, however, we do not assume that the perturbation \mathbf{p} is weak but rather regard \mathbf{p} as a quantity of order $\mathcal{O}(1)$. Instead, we assume that each amplitude r_i is forced to be of order $\mathcal{O}(\epsilon^2)$ with $0 \leq \epsilon^2 \ll 1$ even under the effect of \mathbf{p} , namely, \mathbf{p} is designed such that the amplitude r_i does not deviate largely from 0 as we explain later. In this case, we have $\mathbf{X} = \chi(\theta) + \mathcal{O}(\epsilon^2)$ with $\theta = \Theta(\mathbf{X})$, $\nabla\Theta(\mathbf{X}) = \nabla\Theta(\mathbf{X})|_{\mathbf{X}=\chi(\theta)} + \mathcal{O}(\epsilon^2)$, $\nabla R_i(\mathbf{X}) = \nabla R_i(\mathbf{X})|_{\mathbf{X}=\chi(\theta)} + \mathcal{O}(\epsilon^2)$, and $\mathbf{p}(\mathbf{X}, t) = \mathbf{p}(\chi(\theta), t) + \mathcal{O}(\epsilon^2)$. We thus obtain

$$\begin{aligned}\dot{\theta} &= \omega + \langle \mathbf{Z}(\theta), \mathbf{p}(\chi(\theta), t) \rangle + \mathcal{O}(\epsilon^2), \\ \dot{r}_i &= \lambda_i r_i + \langle \mathbf{I}_i(\theta), \mathbf{p}(\chi(\theta), t) \rangle + \mathcal{O}(\epsilon^2),\end{aligned}\tag{7}$$

and neglecting the terms of order $\mathcal{O}(\epsilon^2)$ leads to the lowest-order phase-amplitude equation in the same form as Eq. (6).

It often happens that the negative real part of λ_i decreases quickly with i and only the first few amplitude variables r_i for $i = 1, \dots, M$ decay slowly. We can then neglect fast-decaying amplitudes and reduce the dimensionality of the system from N to $M + 1$, i.e., to a phase equation for θ and the first M amplitude equations for r_i . Thus, we obtain reduced

$(M + 1)$ -dimensional phase-amplitude equations from the original N -dimensional system near χ . The phase equation is characterized by the natural frequency ω and PSF $\mathbf{Z}(\theta)$, and similarly the amplitude equations are characterized by the Floquet exponents λ_i and ISFs $\mathbf{I}_i(\theta)$ for $i = 1, \dots, M$. In the simplest situation, we may need to consider only the slowest-decaying amplitude r_1 when λ_1 is real, or only a pair of slowest-decaying amplitudes r_1 and r_2 when $\lambda_1 = \lambda_2^*$ is complex, and reduce the dimensionality of the original N -dimensional system to $M + 1 = 2$ or 3 .

From the phase and amplitudes θ and r_i , the original system state can be approximately reconstructed as $\mathbf{X} \approx \boldsymbol{\chi}(\theta)$ at the lowest order, or

$$\mathbf{X} \approx \boldsymbol{\chi}(\theta) + \sum_{i=1}^M r_i \mathbf{u}_i(\theta/\omega) \quad (8)$$

at the first order, where $\mathbf{u}_i(t)$ is the right Floquet eigenvector associated with λ_i introduced in the next subsection.

In the lowest-order phase-amplitude reduction introduced here, the phase equation is independent of the amplitudes whereas the amplitude equations depend on the phase. Thus, the amplitude equations are not necessary if we are only interested in the phase dynamics of the oscillator, provided that the perturbation given to the oscillator is sufficiently weak. In this study, we do not assume the perturbation to be weak and we explicitly use the amplitude equations to suppress deviations of the system state from the limit cycle.

B. Floquet theory

Though it is difficult to obtain the phase and amplitude functions Θ and R_i analytically, the PSF and ISFs are given by the left Floquet eigenvectors of the limit cycle and can be evaluated numerically^{8–11,20,22,52,54,60,61}.

By linearizing the unperturbed system Eq. (1) around the limit-cycle solution $\mathbf{X}_0(t)$ for a small variation $\mathbf{y}(t) = \mathbf{X}(t) - \mathbf{X}_0(t) \in \mathbb{R}^N$, we obtain a periodically driven linear system, $\dot{\mathbf{y}}(t) = \mathbf{J}(\mathbf{X}_0(t))\mathbf{y}(t)$, where $\mathbf{J} \in \mathbb{R}^{N \times N}$ is a T -periodic Jacobian matrix of \mathbf{F} evaluated at $\mathbf{X} = \mathbf{X}_0(t)$. We denote the fundamental matrix of this linearized equation as $\boldsymbol{\Psi}(t) \in \mathbb{R}^{N \times N}$, which satisfies $\dot{\boldsymbol{\Psi}}(t) = \mathbf{J}(\mathbf{X}_0(t))\boldsymbol{\Psi}(t)$ with an initial condition $\boldsymbol{\Psi}(0) = \mathbf{E}$, where $\mathbf{E} \in \mathbb{R}^{N \times N}$ is an identity matrix^{62,63}.

According to the Floquet theory, $\boldsymbol{\Psi}(t)$ can be expressed as $\boldsymbol{\Psi}(t) = \mathbf{P}(t) \exp(\boldsymbol{\Lambda}t)$ where \mathbf{P}

is a T -periodic matrix satisfying $\mathbf{P}(t+T) = \mathbf{P}(t) \in \mathbb{R}^{N \times N}$ and $\mathbf{P}(0) = \mathbf{E}$, and $\mathbf{\Lambda} \in \mathbb{R}^{N \times N}$ is a constant matrix. It is noted that $\mathbf{\Lambda}$ depends on the initial condition $\mathbf{X}_0(0)$ at $t = 0$ of the system. The matrix $\mathbf{M} = \exp(\mathbf{\Lambda}T)$ is called a monodromy matrix^{62,63}.

We consider the eigensystem $\{\lambda_i \in \mathbb{C}, \mathbf{u}_i \in \mathbb{C}^N, \mathbf{v}_i \in \mathbb{C}^N\}_{i=0,1,\dots,N-1}$ of $\mathbf{\Lambda}$ satisfying $\mathbf{\Lambda}\mathbf{u}_i = \lambda_i\mathbf{u}_i$ and $\mathbf{\Lambda}^\dagger\mathbf{v}_i = \lambda_i^*\mathbf{v}_i$ for $i = 0, \dots, N-1$, where \dagger represents Hermitian conjugate (transpose for real matrices). The eigenvalue λ_i gives i th Floquet exponent (i.e., $e^{\lambda_i T}$ is the Floquet multiplier; the principal value is chosen when λ_i is complex) and we call the associated right and left eigenvectors \mathbf{u}_i and \mathbf{v}_i the Floquet eigenvectors. Among them, one of the Floquet exponent is $\lambda_0 = 0$ and the associated right Floquet eigenvector \mathbf{u}_0 is parallel to the tangent vector of χ at $\mathbf{X}_0(0)$ ^{9,22}. We choose this vector as $\mathbf{u}_0 = (1/\omega)d\mathbf{X}_0(t)/dt|_{t=0}$, where the factor $(1/\omega)$ is introduced to be consistent with the convention of the phase reduction theory. The eigenvectors are normalized to satisfy the bi-orthonormality relation $\langle \mathbf{v}_i, \mathbf{u}_j \rangle = \delta_{ij}$ for $i, j = 1, \dots, N$.

Using the right and left Floquet eigenvectors \mathbf{u}_i and \mathbf{v}_i , we further define

$$\mathbf{u}_i(t) = \mathbf{P}(t)\mathbf{u}_i \in \mathbb{C}^N, \quad \mathbf{v}_i(t) = (\mathbf{P}(t)^{-1})^\dagger \mathbf{v}_i \in \mathbb{C}^N \quad (i = 0, 1, \dots, N-1) \quad (9)$$

for $0 \leq t < T$ along χ , which we also call the Floquet eigenvectors. These eigenvectors are T -periodic, i.e., $\mathbf{u}_i(T) = \mathbf{u}_i(0) = \mathbf{u}_i$ and $\mathbf{v}_i(T) = \mathbf{v}_i(0) = \mathbf{v}_i$, and satisfy the bi-orthonormality relation $\langle \mathbf{v}_i(t), \mathbf{u}_j(t) \rangle = \delta_{i,j}$ ($i, j = 0, 1, \dots, N-1$) for $0 \leq t < T$. We can also confirm that these vectors are T -periodic solutions to the following set of linear and adjoint linear equations^{22,54,60,61}:

$$\begin{aligned} \frac{d}{dt}\mathbf{u}_i(t) &= (\mathbf{J}(\mathbf{X}_0(t)) - \lambda_i)\mathbf{u}_i(t), \\ \frac{d}{dt}\mathbf{v}_i(t) &= -(\mathbf{J}(\mathbf{X}_0(t))^\dagger - \lambda_i^*)\mathbf{v}_i(t). \end{aligned} \quad (10)$$

The PSF and ISFs, which are the gradients of the phase and amplitude functions $\Theta(\mathbf{X})$ and $R_i(\mathbf{X})$ evaluated at $\mathbf{X} = \chi(\theta)$ with $\theta = \omega t$ on the limit cycle χ , can be expressed by the left Floquet eigenvectors $\mathbf{v}_i(t)$ ($i = 0, 1, \dots, N-1$) as

$$\begin{aligned} \mathbf{Z}(\theta) &= \nabla\Theta|_{\mathbf{X}=\chi(\theta)} = \mathbf{v}_0(\theta/\omega), \\ \mathbf{I}_i(\theta) &= \nabla R_i|_{\mathbf{X}=\chi(\theta)} = \mathbf{v}_i(\theta/\omega), \end{aligned} \quad (11)$$

for $0 \leq \theta < 2\pi$. Indeed, assuming that the above relations hold, we can linearly approximate

the phase and amplitude functions for \mathbf{X} close to $\chi(\theta)$ as

$$\begin{aligned}\Theta(\mathbf{X}) &\approx \Theta(\chi(\theta)) + \langle \nabla \Theta|_{\mathbf{X}=\chi(\theta)}, \mathbf{y}(t) \rangle = \theta + \langle \mathbf{v}_0(t), \mathbf{y}(t) \rangle, \\ R_i(\mathbf{X}) &\approx R_i(\chi(\theta)) + \langle \nabla R_i|_{\mathbf{X}=\chi(\theta)}, \mathbf{y}(t) \rangle = \langle \mathbf{v}_i(t), \mathbf{y}(t) \rangle,\end{aligned}\tag{12}$$

for sufficiently small $\mathbf{y}(t) = \mathbf{X}(t) - \chi(\theta(t))$. We then have

$$\begin{aligned}\frac{d}{dt}\Theta(\mathbf{X}) &\approx \frac{d\theta}{dt} + \left\langle \frac{d\mathbf{v}_0(t)}{dt}, \mathbf{y}(t) \right\rangle + \left\langle \mathbf{v}_0(t), \frac{d\mathbf{y}(t)}{dt} \right\rangle \\ &= \omega + \left\langle \frac{d\mathbf{v}_0(t)}{dt}, \mathbf{y}(t) \right\rangle + \langle \mathbf{v}_0(t), \mathbf{J}(\mathbf{X}_0(t))\mathbf{y}(t) \rangle \\ &= \omega + \left\langle \frac{d\mathbf{v}_0(t)}{dt} + \mathbf{J}(\mathbf{X}_0(t))^\dagger \mathbf{v}_0(t), \mathbf{y}(t) \right\rangle = \omega\end{aligned}\tag{13}$$

and

$$\begin{aligned}\frac{d}{dt}R_i(\mathbf{X}) &\approx \left\langle \frac{d\mathbf{v}_i(t)}{dt}, \mathbf{y}(t) \right\rangle + \left\langle \mathbf{v}_i(t), \frac{d\mathbf{y}(t)}{dt} \right\rangle \\ &= \left\langle \frac{d\mathbf{v}_i(t)}{dt}, \mathbf{y}(t) \right\rangle + \langle \mathbf{v}_i(t), \mathbf{J}(\mathbf{X}_0(t))\mathbf{y}(t) \rangle \\ &= \left\langle \frac{d\mathbf{v}_i(t)}{dt} + \mathbf{J}(\mathbf{X}_0(t))^\dagger \mathbf{v}_i(t), \mathbf{y}(t) \right\rangle = \langle \lambda_i^* \mathbf{v}_i(t), \mathbf{y}(t) \rangle = \lambda_i R_i(\mathbf{X}),\end{aligned}\tag{14}$$

hence Θ and R_i satisfy their defining equations (2) within the linear approximation. For more details, see e.g. Appendix A in Ref.²².

Thus, by numerically solving the linear and adjoint linear equations (10) and obtaining $\mathbf{u}_i(t)$ and $\mathbf{v}_i(t)$, we can calculate the PSF $\mathbf{Z}(\theta)$ and ISF $\mathbf{I}_i(\theta)$ and use them to reduce the original N -dimensional dynamical system given by Eq. (1) to the $(M+1)$ -dimensional phase and amplitude equations (7). Details of the numerical schemes for calculating the Floquet eigenvectors are explained in Appendix B.

III. OPTIMAL ENTRAINMENT WITHOUT AMPLITUDE SUPPRESSION

In this section, we briefly review the optimization of the periodic input for linear stability within the phase-reduction framework by Zlotnik *et al.*³⁷. We also demonstrate that the method fails when the periodic input is too strong due to breakdown of the phase-only approximation, leading to discrepancy between the target and realized phase-locking points.

We consider a limit-cycle oscillator subjected to a periodic input described by Eq. (3). The perturbation is given in the form $\mathbf{p}(t) = \mathbf{q}(\Omega t)$, where \mathbf{q} represents the waveform of the periodic input of frequency Ω and period $T_e = 2\pi/\Omega$. The aim of this method is to derive the optimal waveform for the periodic input. Assuming that \mathbf{q} is of order $\mathcal{O}(\epsilon)$ ($0 \leq \epsilon \ll 1$) and employing the phase reduction, we obtain the following approximate phase equation for the oscillator phase $\theta(t) = \Theta(\mathbf{X})$:

$$\dot{\theta}(t) = \omega + \langle \mathbf{Z}(\theta(t)), \mathbf{q}(\Omega t) \rangle. \quad (15)$$

We also assume that the frequency mismatch $\Delta = \omega - \Omega$ between the oscillator and the input frequency is sufficiently small and of order $\mathcal{O}(\epsilon)$. Then the phase difference $\phi(t) = \theta(t) - \Omega t$ between the oscillator and the periodic input obeys

$$\dot{\phi}(t) = \Delta + \langle \mathbf{Z}(\phi(t) + \Omega t), \mathbf{q}(\Omega t) \rangle. \quad (16)$$

The right-hand side of Eq. (16) is of order $\mathcal{O}(\epsilon)$ and hence $\phi(t)$ evolves much more slowly than \mathbf{q} . We can thus apply the averaging approximation^{9,64} to obtain

$$\dot{\phi} = \Delta + \Gamma(\phi), \quad (17)$$

where $\Gamma(\phi) = [\langle \mathbf{Z}(\phi + \Omega t), \mathbf{q}(\Omega t) \rangle]_t$ is the phase coupling function and $[\cdot]_t = \frac{1}{T_e} \int_0^{T_e} (\cdot) dt$ represents a time average over one input period T_e .

We seek the optimal input for which (i) a given ϕ^* ($0 \leq \phi < 2\pi$) is a stable phase-locking point and (ii) the linear stability (negative of the stability exponent) at ϕ^* ,

$$-\Gamma'(\phi^*) = -[\langle \mathbf{Z}'(\phi^* + \Omega t), \mathbf{q}(\Omega t) \rangle]_t, \quad (18)$$

is maximized under a constraint on the power of the periodic input \mathbf{q} . This maximization problem is formulated as

$$\begin{aligned} & \max_{\mathbf{q}} -\Gamma'(\phi^*), \\ \text{s.t. } & \Delta + \Gamma(\phi^*) = 0, \quad [\|\mathbf{q}\|^2]_t = P, \end{aligned} \quad (19)$$

where the one-period average of the power $\|\mathbf{q}\|^2 = \langle \mathbf{q}, \mathbf{q} \rangle$ of the input is constrained at a constant $P > 0$. These constraints can be incorporated into the Lagrange function

$$C(\mathbf{q}, \mu, \nu) = -\Gamma'(\phi^*) + \mu\{\Delta + \Gamma(\phi^*)\} + \nu(P - [\|\mathbf{q}\|^2]_t) \quad (20)$$

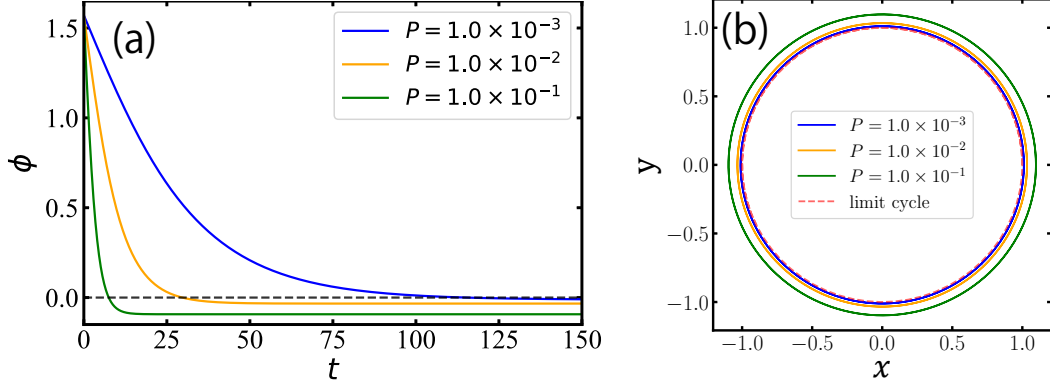


FIG. 1. Results of phase-only optimization for the linear stability. (a) Evolution of the phase differences. (b) Trajectories on the phase plane in the steady state for input powers $P = 1.0 \times 10^{-3}$ (blue), 1.0×10^{-2} (yellow), and 1.0×10^{-1} (green). Black dashed line in (a) indicates the target phase difference $\phi^* = 0$, and the red dashed curve in (b) shows the unperturbed limit cycle with $P = 0$.

by introducing Lagrange multipliers μ and ν . From the conditions for the extremum, we obtain an Euler-Lagrange equation and two additional conditions as follows:

$$\frac{\delta C}{\delta \mathbf{q}} = \frac{1}{T_e} \{-\mathbf{Z}'(\phi^* + \Omega t) + \mu \mathbf{Z}(\phi^* + \Omega t) - 2\nu \mathbf{q}(\Omega t)\} = 0, \quad (21)$$

$$\frac{\partial C}{\partial \mu} = \Delta + [\langle \mathbf{Z}(\phi^* + \Omega t), \mathbf{q}(\Omega t) \rangle]_t = 0, \quad (22)$$

$$\frac{\partial C}{\partial \nu} = P - [\|\mathbf{q}(\Omega t)\|^2]_t = 0, \quad (23)$$

where $\delta/\delta \mathbf{q}$ represents functional differentiation with respect to \mathbf{q} . The optimal input waveform in the phase-reduction framework, denoted as $\mathbf{q}^{ls}(\Omega t)$, is thus obtained as

$$\mathbf{q}^{ls}(\Omega t) = -\frac{1}{2\nu} \mathbf{Z}'(\phi^* + \Omega t) + \frac{\mu}{2\nu} \mathbf{Z}(\phi^* + \Omega t), \quad (24)$$

$$\mu = -\frac{2\nu \Delta}{[\|\mathbf{Z}\|^2]_t}, \quad \nu = \frac{1}{2} \sqrt{\frac{[\|\mathbf{Z}'\|^2]_t}{P - \frac{\Delta^2}{[\|\mathbf{Z}\|^2]_t}}}. \quad (25)$$

In the above optimization, we assumed that the intensity P of the periodic input is sufficiently small. Here, we illustrate the breakdown of the phase-only approximation for large P , which leads to a discrepancy between the target and realized phase-locking points.

We use the Stuart-Landau oscillator, a normal form of the supercritical Hopf bifurcation^{9,20}, as an example, given by

$$\begin{pmatrix} \dot{x} \\ \dot{y} \end{pmatrix} = \begin{pmatrix} x - ay - (x - by)(x^2 + y^2) \\ ax + y - (bx + y)(x^2 + y^2) \end{pmatrix}. \quad (26)$$

We assume the parameter values to be $a = 2$ and $b = 1$, which gives a natural frequency $\omega = a - b = 1$. The input frequency is assumed to be equal to the natural frequency, $\Omega = 1$. The target phase-locking point is set as $\phi^* = 0$ and the initial condition of (x, y) is chosen such that the phase difference at $t = 0$ is $\phi(0) = \pi/2$.

Figures 1(a) and (b) show the evolution of the phase difference $\phi(t)$ and the trajectory on the (x, y) phase plane, respectively, for three values of P . From Fig. 1(a), we observe that the convergence becomes faster as P is increased, but the realized phase-locking point deviates more significantly from the target point $\phi^* = 0$. This discrepancy is caused by the breakdown of the phase-only approximation. As shown in Fig. 1(b), as the intensity of the input P increases, the system state deviates from the unperturbed limit cycle more significantly, yielding larger errors in the phase reduction and invalidating the results of the optimization.

IV. OPTIMAL ENTRAINMENT WITH AMPLITUDE SUPPRESSION

From the results in the previous section, it is expected that faster convergence to the target phase-locking point can be achieved by applying stronger periodic inputs while suppressing the amplitude deviations of the system state from the limit cycle. To accomplish this, we propose two methods: an amplitude-feedback method and an amplitude-penalty method.

A. Amplitude-feedback method

The first method is to add an amplitude-feedback term to the optimal input \mathbf{q}^{ls} derived in the previous section. We consider a modified periodic input given by

$$\mathbf{q}^{fb}(t) = \mathbf{q}^{ls}(\Omega t) - \alpha \mathbf{y}(t) \quad (27)$$

where $\mathbf{y}(t) = \mathbf{X} - \boldsymbol{\chi}(\theta(t))$ represents the deviation of the system state from the limit cycle $\boldsymbol{\chi}$ and $\alpha > 0$ is a feedback gain. When $\mathbf{y}(t)$ is small, we can approximately expand it as

$$\mathbf{y}(t) \approx \sum_{i=1}^M r_i(t) \mathbf{u}_i(\theta(t)/\omega) \quad (28)$$

by using the first M amplitude variables r_i for $i = 1, \dots, M$ ($M \leq N - 1$). Therefore, the phase and amplitude equations become

$$\begin{aligned} \dot{\theta}(t) &= \omega + \langle \mathbf{Z}(\theta(t)), \mathbf{q}^{fb}(t) \rangle \\ &= \omega + \langle \mathbf{Z}(\theta(t)), \mathbf{q}^{ls}(\Omega t) \rangle \end{aligned} \quad (29)$$

and

$$\begin{aligned} \dot{r}_i(t) &= \lambda_i r_i(t) + \langle \mathbf{I}_i(\theta(t)), \mathbf{q}^{fb}(t) \rangle \\ &= (\lambda_i - \alpha) r_i(t) + \langle \mathbf{I}_i(\theta(t)), \mathbf{q}^{ls}(\Omega t) \rangle \end{aligned} \quad (30)$$

from the bi-orthonormality relation of the left Floquet eigenvectors (PSF and ISFs) and the right Floquet eigenvectors, $\langle \mathbf{Z}(\theta), \mathbf{u}_i(\theta/\omega) \rangle = 0$ and $\langle \mathbf{I}_i(\theta), \mathbf{u}_j(\theta/\omega) \rangle = \delta_{ij}$ for $i = 1, \dots, M$. Namely, at the lowest-order phase-amplitude reduction, the phase dynamics is unaffected by the feedback while the convergence rate of the amplitude r_i changes from λ_i to $\lambda_i - \alpha$. We thus expect faster decay of the amplitudes and suppression of the deviation of the system state from the unperturbed limit cycle $\boldsymbol{\chi}$.

B. Amplitude-penalty method

The second method, which is feedforward, is to add a penalty term to the optimization problem, Eq. (19), which increases if the amplitude deviations of the system state from the limit cycle are excited. Specifically, we consider the following optimization problem:

$$\begin{aligned} \max_{\mathbf{q}} \quad & -\Gamma'(\phi^*) - \sum_{i=1}^M k_i [\langle \mathbf{I}_i(\phi^* + \Omega t), \mathbf{q}(\Omega t) \rangle^2]_t, \\ \text{s.t.} \quad & \Delta + \Gamma(\phi^*) = 0, \quad [\|\mathbf{q}\|^2]_t = P, \end{aligned} \quad (31)$$

where the second term in the objective function represents the penalty and $k_i \geq 0$ gives the weight of the penalty for the excitation of the i th amplitude. We use the same weights $k_i = k_{i+1}$ if the i th and $i + 1$ th amplitudes are mutually complex conjugate, namely, when

$\lambda_i = \lambda_{i+1}^*$. The inner product $\langle \mathbf{I}_i(\phi^* + \Omega t), \mathbf{q}(\Omega t) \rangle$ is nothing but the second perturbation term in the amplitude equation (6) for the case that the oscillator phase is $\theta = \phi^* + \Omega t$ and the input phase is Ωt ; namely, the effect that the periodic input exerts on the i th amplitude when the oscillator is phase-locked to the periodic input at the target phase difference ϕ^* .

To solve the above optimization problem, we introduce a Lagrange function

$$C(\mathbf{q}, \mu, \nu) = -\Gamma'(\phi^*) - \sum_{i=1}^M k_i [\langle \mathbf{I}_i(\phi^* + \Omega t), \mathbf{q}(\Omega t) \rangle^2]_t + \mu(\Delta + \Gamma(\phi^*)) + \nu(P - [\|\mathbf{q}\|^2]_t), \quad (32)$$

where μ and ν are the Lagrange multipliers and the amplitudes up to M ($\leq N - 1$) are taken into account. The conditions for the extremum yield

$$\frac{\delta C}{\delta \mathbf{q}} = \frac{1}{T_e} \left\{ -\mathbf{Z}'(\phi^* + \Omega t) - 2 \sum_{i=1}^M k_i \mathbf{I}_i(\phi^* + \Omega t) \mathbf{I}_i^\dagger(\phi^* + \Omega t) \mathbf{q}(\Omega t) + \mu \mathbf{Z}(\phi^* + \Omega t) - 2\nu \mathbf{q}(\Omega t) \right\} = 0, \quad (33)$$

$$\frac{\partial C}{\partial \mu} = \Delta + [\langle \mathbf{Z}(\phi^* + \Omega t), \mathbf{q}(\Omega t) \rangle]_t = 0, \quad (34)$$

$$\frac{\partial C}{\partial \nu} = P - [\|\mathbf{q}(\Omega t)\|^2]_t = 0. \quad (35)$$

From Eq. (33), we obtain

$$\mathbf{q}(\Omega t) = \frac{1}{2} \left\{ \nu \mathbf{E} + \sum_{i=1}^M k_i \mathbf{I}_i(\phi^* + \Omega t) \mathbf{I}_i^\dagger(\phi^* + \Omega t) \right\}^{-1} \{ -\mathbf{Z}'(\phi^* + \Omega t) + \mu \mathbf{Z}(\phi^* + \Omega t) \}, \quad (36)$$

where $\mathbf{E} \in \mathbb{R}^{N \times N}$ is an identity matrix. By plugging Eq. (36) into Eq. (34), we obtain

$$\Delta + \left[\left\langle \mathbf{Z}, \frac{1}{2} \left\{ \nu \mathbf{E} + \sum_{j=1}^M k_j \mathbf{I}_j \mathbf{I}_j^\dagger \right\}^{-1} \{ -\mathbf{Z}' + \mu \mathbf{Z} \} \right\rangle \right]_t = 0, \quad (37)$$

from which the relation between μ and ν is derived as

$$\mu = \frac{\left[\left\langle \mathbf{Z}, \{ \nu \mathbf{E} + \sum_{i=1}^M k_i \mathbf{I}_i \mathbf{I}_i^\dagger \}^{-1} \mathbf{Z}' \right\rangle \right]_t - 2\Delta}{\left[\left\langle \mathbf{Z}, \{ \nu \mathbf{E} + \sum_{i=1}^M k_i \mathbf{I}_i \mathbf{I}_i^\dagger \}^{-1} \mathbf{Z} \right\rangle \right]_t}. \quad (38)$$

Though it is difficult to solve this problem analytically, we can numerically find an appropriate Lagrange multiplier ν , which determines μ and \mathbf{q} from Eqs. (36) and (38), such that the power constraint in Eq. (35) is satisfied. We denote the resulting optimal input as \mathbf{q}^{pl} .

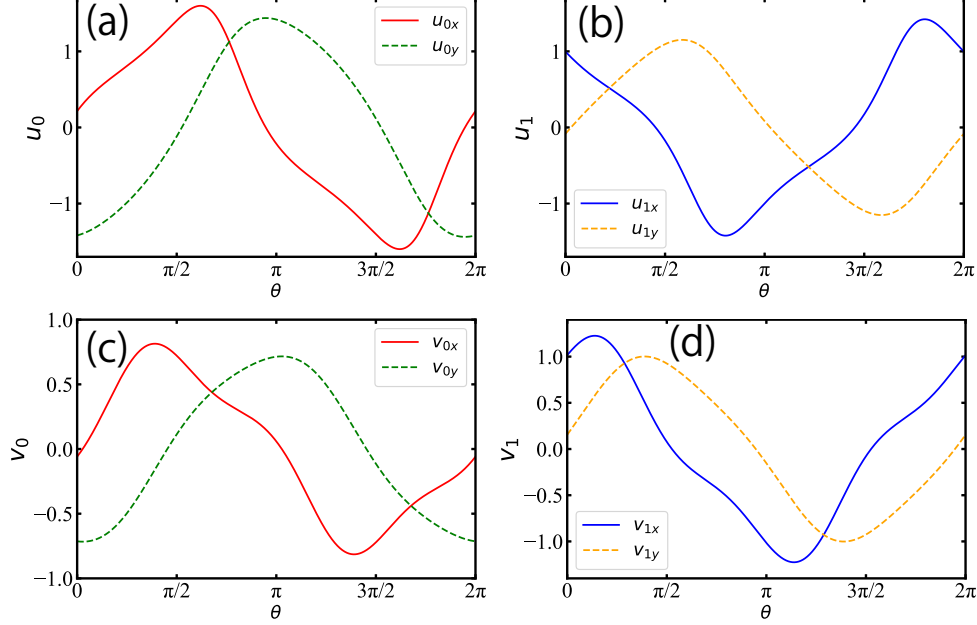


FIG. 2. Floquet eigenvectors $\mathbf{u}_i(\theta/\omega)$, $\mathbf{v}_i(\theta/\omega)$ of the Van der Pol model for $i = 0$ (a,c) and $i = 1$ (b, d). Both x and y components of the eigenvector are shown in each figure.

If we consider the limit $k_i \rightarrow \infty$ ($i = 1, \dots, M$) in Eq. (31), it is expected that the input waveform \mathbf{q} can possess only the tangential component along the limit cycle because \mathbf{q} should not excite the amplitude deviations at all. In Appendix B, we present the result of optimization for such a tangential input and compare it with the results of the amplitude-penalty method.

V. EXAMPLES

In this section, we illustrate the results of the two methods using a two-dimensional Van der Pol model^{65,66} with a real non-zero Floquet exponent and a three-dimensional Willamowski-Rössler model⁶⁷ that possesses a pair of complex non-zero Floquet exponents.

A. Van der Pol model

The Van der Pol model of an electric oscillator is given by^{65,66}

$$\begin{pmatrix} \dot{x} \\ \dot{y} \end{pmatrix} = \begin{pmatrix} ax - x^3/3 - y \\ x \end{pmatrix}, \quad (39)$$

where x and y represent the current and voltage, respectively, and a is a control parameter, which we fix as $a = 0.5$. The natural frequency of the limit cycle is $\omega \approx 0.985$ and the non-zero Floquet exponent is $\lambda_1 \approx -0.508$. The Floquet eigenvectors are plotted in Fig. 2 (See Appendix B for the numerical methods). We fix the input power as $P = 0.01$ and the input frequency as $\Omega = \omega + 0.05 = 1.035$. It is noted that the value $P = 0.01$ is already non-weak for this system and can excite amplitude deviations. The target phase-locking point is $\phi^* = 0$ and the initial system state (x, y) at $t = 0$ is chosen such that the initial phase difference is $\phi(0) = \pi/2$. The feedback gain in the amplitude-feedback method is $\alpha = 10$ and the weight in the amplitude-penalty method is $k_1 = 100$ (note that $N = 2$).

The results of the optimal entrainment with the amplitude-feedback method are shown in Figs. 3(a) and (b). The phase difference ϕ converges to the correct target value $\phi^* = 0$ when the amplitude feedback is applied. This is because the deviation of the system state from the unperturbed limit cycle is suppressed as shown in Fig. 3(b) and the validity of the phase approximation is kept. In contrast, without the feedback, ϕ converges to an incorrect value due to non-negligible amplitude deviations of the system state from the limit cycle.

The results of the optimal entrainment with the amplitude-penalty method are shown in Figs. 3(c), (d), and (e). The phase difference converges to the correct target value also in this case when the penalty is introduced. This is because the optimal input with the amplitude penalty does not excite the amplitude deviations and the system state stays near the unperturbed limit cycle as shown in Fig. 3(d). In contrast, without the penalty, ϕ converges to an incorrect value due to the amplitude deviations.

In Fig. 3(c), the convergence is slower in the case with the penalty than the case without the penalty. This is because some of the vector components that are included in the input waveform without the penalty are dropped in the input waveform with the penalty to avoid excitation of the amplitude deviations, leading to lower linear stability. Figure 3(e) shows the right-hand side of Eq. (17) for the optimal inputs with and without the penalty. The linear stability of the phase-locking point $\phi^* = 0$ is given by the (negative) slope of the curve

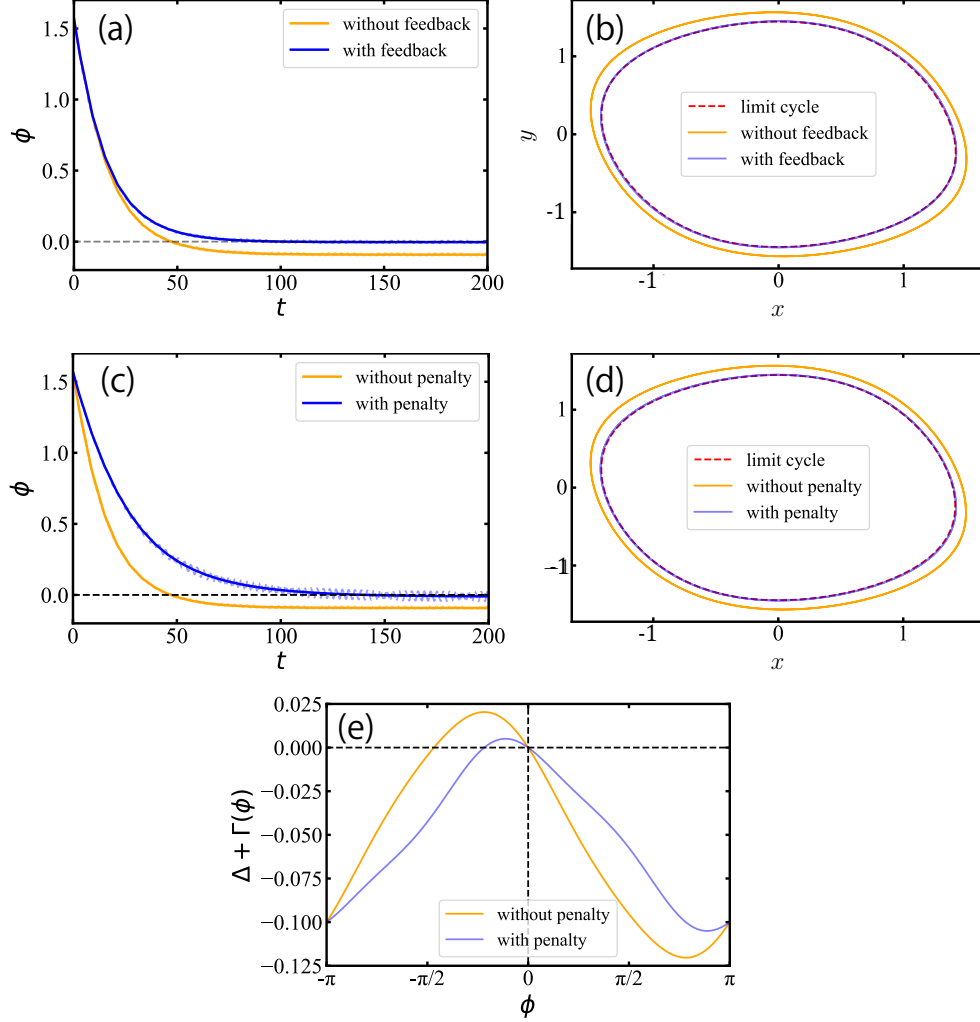


FIG. 3. Results of amplitude-feedback and amplitude-penalty methods for the Van der Pol model. (a) Evolution of the phase differences (raw and averaged) and (b) Trajectory on the phase plane for the amplitude-feedback method. (c) Evolution of the phase differences (raw and averaged) and (d) Trajectory on the phase plane for the amplitude-penalty method. (e) Right-hand side of Eq. (17) for the cases with and without the amplitude penalty. In (a) and (c), the black dashed lines represent the target phase-locking point $\phi^* = 0$. In (b) and (d), the red dashed curves show the unperturbed limit cycle when $P = 0$.

at the origin. The case without the penalty gives higher stability than the case with the penalty if the input is weak, but yields larger amplitude deviations when the input is not weak.

In Figs. 3(a,c), we plotted two values of the phase difference for each curve, that is,

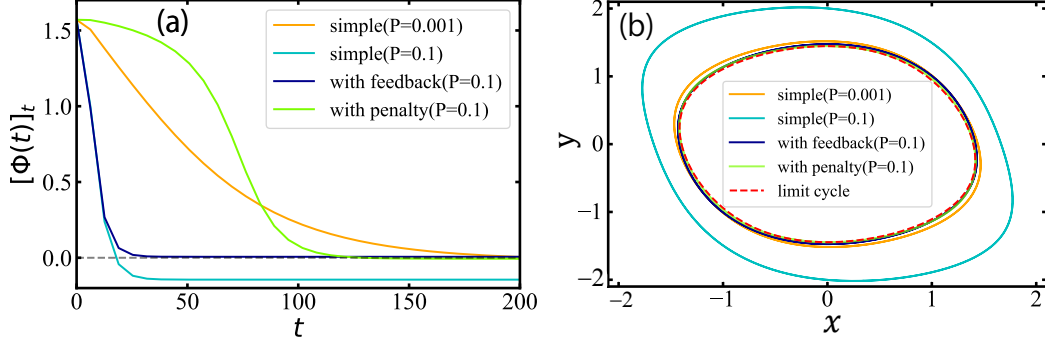


FIG. 4. Optimal entrainment by the amplitude-feedback and amplitude-penalty methods for strong input ($P = 0.1$). For comparison, the cases without feedback nor penalty are also shown for weak ($P = 0.001$) and strong ($P = 0.1$) inputs. (a) Evolution of the phase differences (averaged). (b) Trajectories on the phase plane in the steady state.

the raw values directly measured by using the phase function Θ and the averaged values calculated by taking a moving average of the raw values, where the latter values correspond to the averaged phase variable in Eq. (17) (though we used the same ϕ for both raw and averaged phase variables for simplicity). The raw values for the case with the penalty exhibit small wobbling as the result of the amplitude suppression in this model.

Figure 4 shows the optimal entrainment for the cases with the amplitude feedback ($\alpha = 10$) and with the amplitude penalty ($k = 50$), where the input power $P = 0.1$ is 10 times stronger than that used in Fig. 3 ($P = 0.01$). For comparison, the results without the feedback nor the penalty are also shown as the simple cases for very weak ($P = 0.001$) and strong ($P = 0.1$) inputs. As shown in Fig. 4(a), without the amplitude suppression, the phase difference converges to the correct target value $\phi^* = 0$ only for the weak input ($P = 0.001$) and fails to converge appropriately for the strong input ($P = 0.1$). In contrast, both feedback and penalty methods achieve accurate convergence to the target phase-locking point for the strong input ($P = 0.1$). Figure 4(b) shows that both methods suppress amplitude deviations of the system state from the limit cycle even under the strong input, while the system state largely deviates from the limit cycle for the strong input if neither feedback nor penalty are given. It is remarkable that the proposed methods with the amplitude suppression can achieve much faster convergence to the correct target phase-locking point than the conventional simple method without the amplitude suppression.

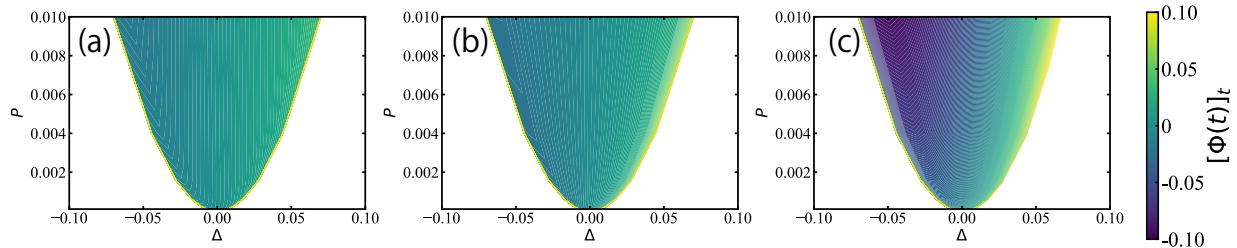


FIG. 5. Arnold tongues and realized phase-locking points for (a) amplitude-feedback method, (b) amplitude-penalty method, and (c) without amplitude suppression. The color map represents the discrepancy between the target phase-locking point $\phi^* = 0$ and the realized phase-locking point.

The amplitude-feedback and amplitude-penalty methods can also widen the parameter region in which the phase difference converges to the correct target phase-locking point. Figure 5 shows the Arnold tongues for the (a) amplitude-feedback method ($\alpha = 2$), (b) amplitude-penalty method ($k = 50$), and (c) without the amplitude suppression. In each figure, the horizontal axis represents the frequency mismatch $\Delta = \omega - \Omega$ and the vertical axis represents the input power P . In each Arnold tongue, the discrepancy between the realized phase-locking point (averaged over one oscillation period after convergence) and the target phase-locking point $\phi^* = 0$ is visualized by a color map. Accurate convergence to $\phi^* = 0$ is confirmed in wide parameter regions in Figs. 5(a) (amplitude-feedback) and 5(b) (amplitude-penalty). In contrast, in the case without the amplitude suppression in Fig. 5(c), the realized phase-locking point shows considerable deviations from $\phi^* = 0$ for large P .

Thus, both proposed methods enable us to apply strong periodic inputs by suppressing the amplitude deviations and achieve much faster entrainment and wider entrainment ranges.

B. Willamowski-Rössler model

The Willamowski-Rössler model for chemical oscillations^{67,68} is described by (in the expression of Ref.⁶⁸)

$$\frac{d}{dt} \begin{pmatrix} x_1 \\ x_2 \\ x_3 \end{pmatrix} = \begin{pmatrix} x_1(b_1 - d_1x_1 - x_2 - x_3) \\ x_2(b_2 - d_2x_2 - x_1) \\ x_3(x_1 - d_3) \end{pmatrix}, \quad (40)$$

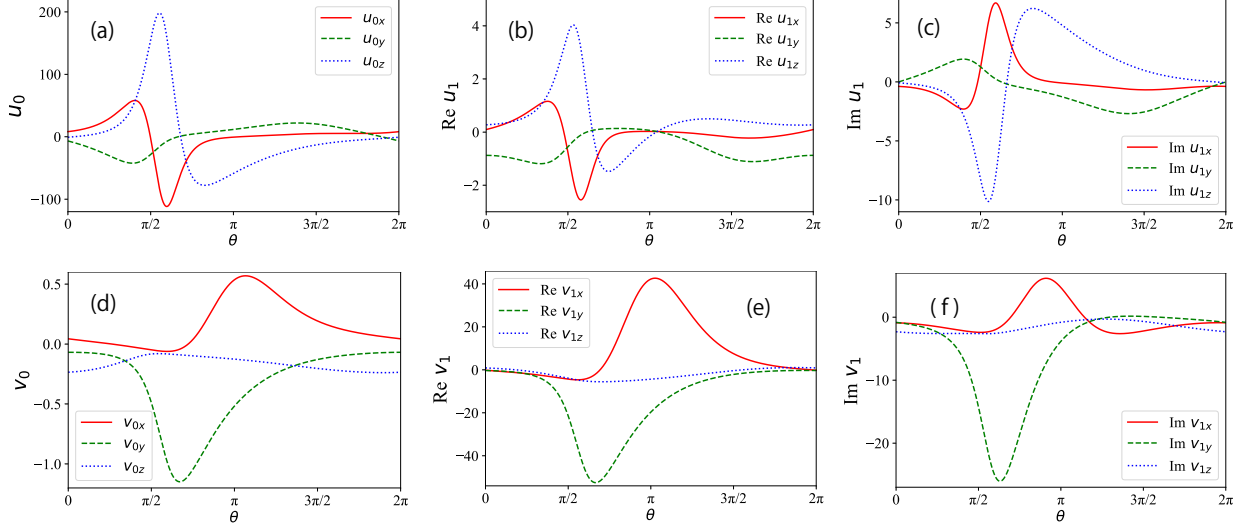


FIG. 6. Floquet eigenvectors $\mathbf{u}_i(\theta/\omega)$, $\mathbf{v}_i(\theta/\omega)$ of the Willamowski-Rössler model for $i = 0$ (a, d) and $i = 1$ (b, e, c, f, real and imaginary parts). Note that the first Floquet eigenvectors are complex and the second Floquet eigenvectors are their complex conjugate, i.e., $\mathbf{u}_2 = \mathbf{u}_1^*$ and $\mathbf{v}_2 = \mathbf{v}_1^*$.

where x_1 , x_2 , and x_3 represent the concentrations of intermediate chemical species and the parameters b_1, b_2, d_1, d_2 , and d_3 are reaction rates. This system has 6 fixed points⁶⁸ and exhibits various dynamics including limit-cycle oscillations and chaos^{69,70}. We set the parameters as $b_1 = 80$, $b_2 = 20$, $d_1 = 0.16$, $d_2 = 0.13$, and $d_3 = 16$, with which the system has a stable limit cycle. The frequency of this limit cycle is $\omega \approx 17.25$ and the non-zero Floquet exponents are given by a pair of complex values $\lambda_1, \lambda_2 \approx -3.280 \pm 4.326\sqrt{-1}$. Figure 6 shows the Floquet eigenvectors $i = 0$ (real) and $i = 1, 2$ (mutually complex conjugate) obtained numerically (see Appendix B for the numerical methods).

We set the input power and frequency as $P = 10$ and $\Omega = \omega + 0.1 = 17.35$, respectively. The target phase-locking point is $\phi^* = 0$ and the initial state is prepared such that the initial phase difference is $\phi(0) = \pi/4$. We use a feedback gain $\alpha = 1.0 \times 10^3$ for the amplitude-feedback method and weights $k_1 = k_2 = 0.1$ for the amplitude-penalty method ($N = 3$).

Figures 7(a) and (b) show the optimal entrainment with the amplitude-feedback method. As shown in Fig. 7(a), the phase difference ϕ converges to the correct target phase-locking point $\phi^* = 0$, because the deviations of the system state from the unperturbed limit cycle is suppressed as shown in Fig. 7(b) and hence the phase equation remains valid. In contrast, without the feedback, the system state deviates from the limit cycle and the phase difference

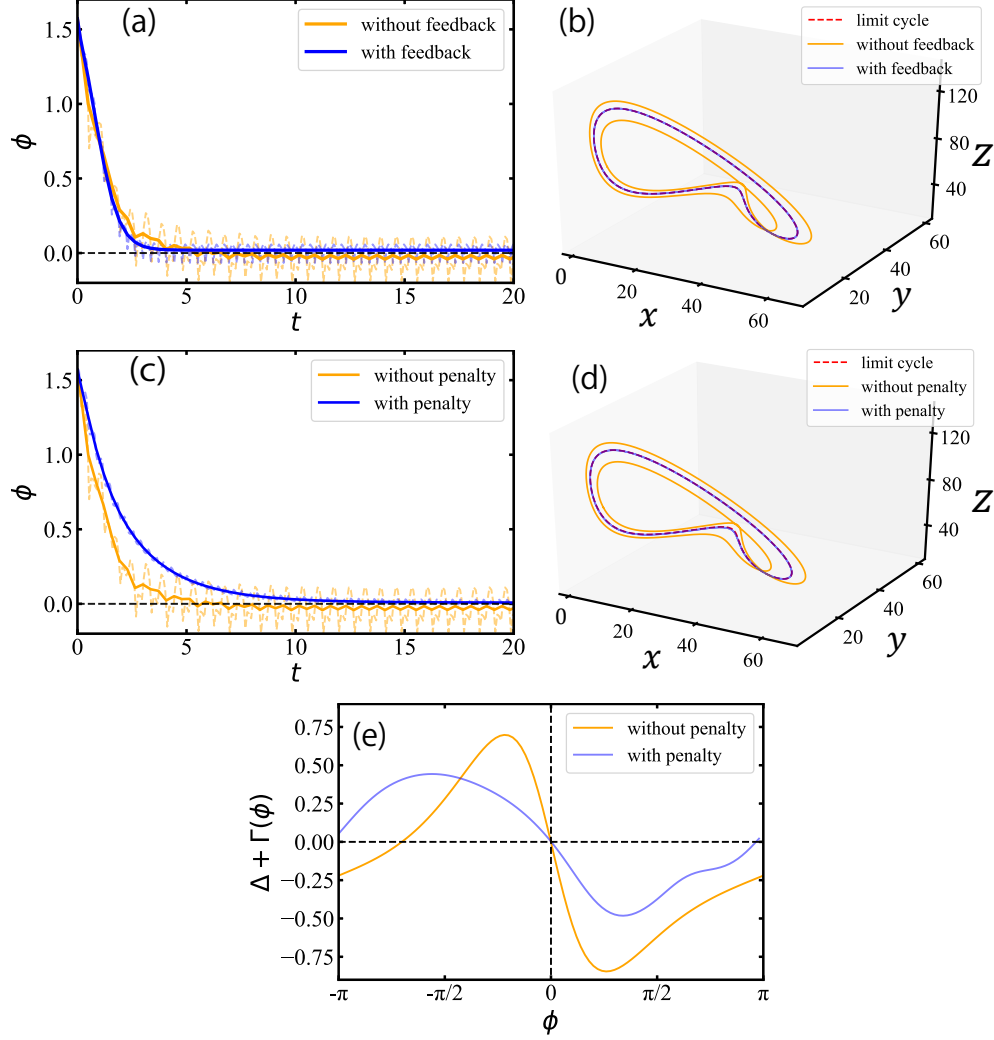


FIG. 7. Results of amplitude-feedback and amplitude-penalty methods for the Willamowski-Rössler model. (a) Evolution of the phase differences (raw and averaged) and (b) Trajectories on the phase plane for the amplitude-feedback method. (c) Evolution of the phase differences (raw and averaged) and (d) Trajectories on the phase plane for the amplitude-penalty method. (e) Right-hand side of Eq. (17) for the cases with and without the amplitude penalty. In (a) and (c), the black dashed lines represent the target phase-locking point $\phi^* = 0$. In (b) and (d), the red dotted lines represent the unperturbed limit cycle with $P = 0$.

does not accurately converge to $\phi^* = 0$.

Figure 7(c) and (d) show the optimal entrainment with the amplitude-penalty method. We can confirm in Fig. 7(c) that the amplitude deviations are suppressed and the phase difference converges to the correct target phase-locking point in the case with the penalty.

The convergence is slower than the case without the penalty because the optimal input with the penalty is less efficient in stabilizing the target phase-locking point in order to suppress the excitation of the amplitude deviations, as can be seen from Fig. 7(e) showing the right-hand side of Eq. (17) with and without the penalty.

In this model, without the amplitude suppression, the raw phase differences exhibit strong wobbling as shown in Figs. 7(a) and (c). This is caused by the considerable deviations of the system state from the unperturbed limit cycle due to strong inputs as shown in Figs. 7(b) and (d). Both the amplitude-feedback and amplitude-penalty methods suppress the wobbling in the phase differences in this model, in contrast to the case for the Van der Pol model. This is because the phase and amplitude directions are generally not orthogonal (only bi-orthogonal) and the suppression of the amplitude deviations also affects the phase dynamics in this case.

VI. DISCUSSION

In this paper, based on the phase-amplitude reduction, we have proposed two methods to obtain input waveforms for fast optimal entrainment of limit-cycle oscillators, namely, the amplitude-feedback and amplitude-penalty methods. We used the Van der Pol and Willamowski-Rössler models as examples and demonstrated that both methods enable us to apply stronger inputs while avoiding the breakdown of the phase approximation, thereby realizing much faster accurate convergence to the target phase-locking point and wider locking range than the conventional method without the amplitude suppression.

The amplitude-feedback method assumes that we can always obtain the phase value of the system, which could be difficult in practical implementation. Development of efficient methods to estimate the system's phase from a small number of measurements would thus be desirable. Regarding the amplitude-penalty method, it considers only the local amplitude deviations at the target phase-locking point. Thus, it only guarantees that the system state is close to the unperturbed limit cycle in the steady entrained state and not in the transient. It would thus be desirable to devise a method that can suppress also the amplitude deviations in the whole transient process for a more general, global optimization.

The methods proposed in the present study can also be used in different types of problems and allow us to apply stronger inputs to the oscillator for fast synchronization and

entrainment. For example, we will be able to use the present method for minimizing the control power of oscillators^{30–33} or maximizing the locking range of periodically driven oscillators^{34–36}. We will also be able to use the present methods for optimizing mutual synchronization of coupled oscillators. Moreover, though we considered only the optimization of the local linear stability of the phase-locked state, we may be able to use the present methods to other optimization problems, such as those for global entrainment property⁴⁵ and phase-distribution control^{42–45}. Finally, using the phase-amplitude reduction frameworks for time-delayed⁵⁶ and spatially-extended⁵⁷ systems, we would also be able to realize fast entrainment in such non-conventional infinite-dimensional systems via amplitude suppression. We thus expect broad applicability of the proposed methods in the control of limit-cycling dynamics using strong perturbations.

ACKNOWLEDGMENTS

This research was funded by JSPS KAKENHI JP17H03279, JP18H03287, JPJSBP120202201, JP20J13778, and JST CREST JP-MJCR1913.

Data availability

The data that supports the findings of this study are available within the article

Appendix A: Tangential periodic input

If we take the limit of large weights in the amplitude-penalty method, i.e., $k_i \rightarrow \infty$ for $i = 1, \dots, M$ in the objective function in Eq. (31), the optimal input waveform is expected to possess only the vector components tangent to the limit cycle. Here, we consider this limit and assume that the input waveform is always proportional to the tangent vector of the limit cycle, optimize its scalar coefficient, and compare the result with those of the amplitude-penalty method.

We assume an input waveform given in the form

$$\mathbf{q}(\Omega t) = \alpha(\Omega t) \mathbf{u}_0((\phi^* + \Omega t)/\omega), \quad (\text{A1})$$

where $\alpha(\Omega t)$ is a temporally periodic scalar coefficient, and consider the following optimization problem for $\alpha(\Omega t)$:

$$\begin{aligned} & \max_{\alpha} -\Gamma'(\phi^*), \\ \text{s.t. } & \Delta + \Gamma(\phi^*) = 0, \quad [\|\alpha(\Omega t)\mathbf{u}_0((\phi^* + \Omega t)/\omega)\|^2]_t = P, \end{aligned} \quad (\text{A2})$$

where the first constraint is for the phase-locking point and the second constraint is for the input power. We introduce Lagrange multipliers μ and ν and consider a Lagrange function

$$C(\alpha, \mu, \nu) = -\Gamma'(\phi^*) + \mu\{\Delta + \Gamma(\phi^*)\} + \nu(P - [\|\alpha(\Omega t)\mathbf{u}_0((\phi^* + \Omega t)/\omega)\|^2]_t). \quad (\text{A3})$$

From the extremum condition, we obtain

$$\frac{\delta C}{\delta \alpha} = -\frac{1}{T_e} \{ \langle \mathbf{Z}'(\phi^* + \Omega t), \mathbf{u}_0((\phi^* + \Omega t)/\omega) \rangle + \mu - 2\nu\alpha(\Omega t)\|\mathbf{u}_0((\Omega t + \phi^*)/\omega)\|^2 \} = 0, \quad (\text{A4})$$

$$\frac{\partial C}{\partial \mu} = \Delta + [\alpha(\Omega t)]_t = 0, \quad (\text{A5})$$

$$\frac{\partial C}{\partial \nu} = P - [\|\alpha(\Omega t)\mathbf{u}_0((\phi^* + \Omega t)/\omega)\|^2]_t = 0, \quad (\text{A6})$$

from which the optimal $\alpha(\Omega t)$ is obtained as

$$\alpha(\Omega t) = \frac{-\langle \mathbf{Z}'(\phi^* + \Omega t), \mathbf{u}_0((\phi^* + \Omega t)/\omega) \rangle + \mu}{2\nu\|\mathbf{u}_0\|^2}, \quad (\text{A7})$$

$$\mu = \left(\left[\frac{\langle \mathbf{Z}', \mathbf{u}_0 \rangle}{\|\mathbf{u}_0\|^2} \right]_t - 2\nu\Delta \right) / \left[\frac{1}{\|\mathbf{u}_0\|^2} \right]_t, \quad (\text{A8})$$

$$\nu = \sqrt{\frac{-\left[\frac{\langle \mathbf{Z}', \mathbf{u}_0 \rangle}{\|\mathbf{u}_0\|^2} \right]_t^2 + \left[\frac{\langle \mathbf{Z}', \mathbf{u}_0 \rangle^2}{\|\mathbf{u}_0\|^2} \right]_t \left[\frac{1}{\|\mathbf{u}_0\|^2} \right]_t}{4 \left(P \left[\frac{1}{\|\mathbf{u}_0\|^2} \right]_t - \Delta^2 \right)}. \quad (\text{A9})$$

Here, for the existence of the optimal $\alpha(\Omega t)$, the argument inside the square root in Eq. (A9) should be positive, which restricts the allowed ranges of P and Δ .

As an example, we consider the Van der Pol model used in Sec. V. The input power and frequency are $P = 0.01$ and $\Omega = \omega + 0.005 = 0.990$, respectively. The target phase-locking point is $\phi^* = 0$ and the initial state of the system is chosen so that the initial phase difference is $\phi(0) = \pi/2$.

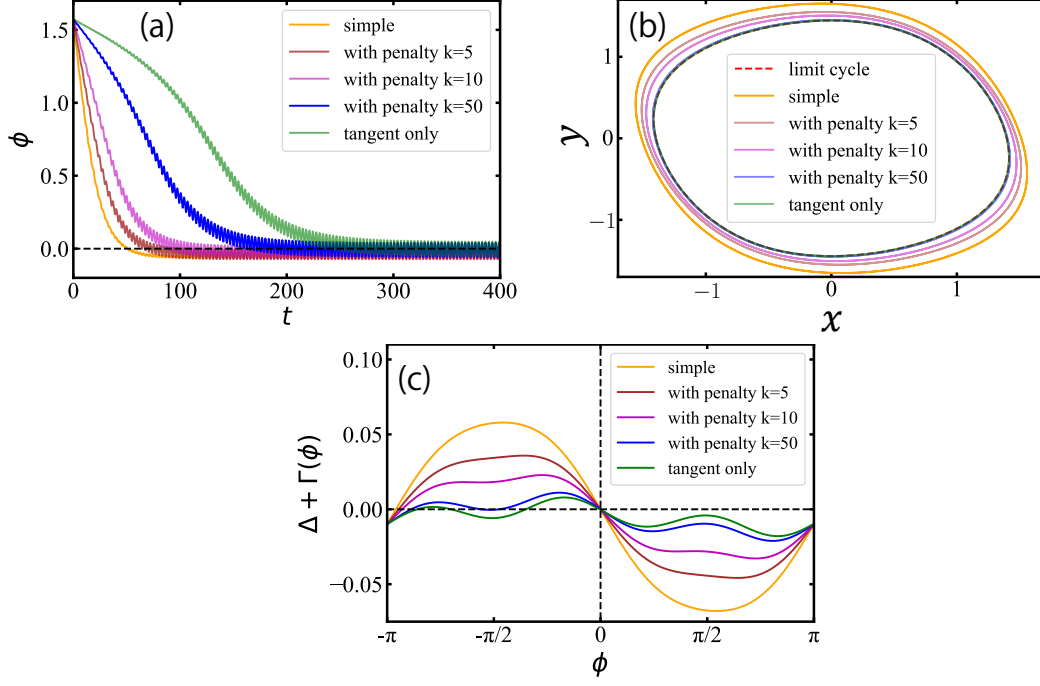


FIG. 8. Optimal entrainment by the tangential input, compared with the amplitude-penalty method for the Van der Pol model. (a) Evolution of the phase differences, (b) Trajectories on the phase plane, (c) Right-hand side of Eq. (17) for the cases without penalty (simple), with penalty ($k = 5, 10, 50$), and tangential input. In (a), black dashed line shows the target phase-locking point $\phi^* = 0$. In (b), red dashed curve shows the unperturbed limit cycle at $P = 0$.

Figure 8 shows the results, where the entrainment by the tangential input is compared with the entrainment by the amplitude-penalty method for several values of the weight $k_1 = k$. The result for the amplitude-penalty method approaches the result for the tangential input as k becomes larger. For relatively small k , including $k = 0$ corresponding to the case without penalty (simple), the phase difference does not converge to the correct target value due to the amplitude deviations as shown in Fig. 8(b). In contrast, for the case with a large amplitude penalty ($k = 50$) and for the tangential case, the amplitude deviations are suppressed or do not arise and the phase difference converges to the correct value, $\phi^* = 0$.

It is notable that the convergence in the tangential case is slower than in the case with the amplitude penalty. This is because the optimal direction of the input waveform for stable entrainment generally possesses vector components in the amplitude directions, though of course too strong amplitude excitations lead to the breakdown of phase-only approximation.

Thus, restricting the directions of the input waveform completely in the tangential direction hampers the realization of larger stability and leads to slower convergence. Allowing small but not too-large amplitude excitations is thus helpful for fast entrainment.

Appendix B: Numerical methods for Floquet exponents and eigenvectors

In this section, we explain the details of the numerical method used to calculate the Floquet eigenvalues and eigenvectors, including the case with complex eigenvalues. The eigenvalues and eigenvectors are calculated in the increasing order of i from $i = 0$.

1. Eigenvector for $i = 0$

The zeroth eigenvalue is $\lambda_0 = 0$. The associated right eigenvector $\mathbf{u}_0(t)$ can be taken as the tangent vector along the limit cycle⁹, i.e.,

$$\mathbf{u}_0(t) = \frac{1}{\omega} \frac{d\mathbf{X}_0(t)}{dt} = \frac{1}{\omega} \mathbf{F}(\mathbf{X}_0(t)), \quad (\text{B1})$$

where the length scale of $\mathbf{u}_0(t)$ is chosen to be consistent with the convention of the phase reduction theory. The zeroth left eigenvector $\mathbf{v}_0(t)$, which is equivalent to the PSF, can be calculated by the adjoint method^{20,61}, namely, by backward integration of the adjoint linear equation

$$\frac{d\mathbf{y}(t)}{dt} = -\mathbf{J}(\mathbf{X}_0(t))^\dagger \mathbf{y}(t) \quad (\text{B2})$$

from an arbitrary final condition. Since $\lambda_0 = 0 > \text{Re } \lambda_1 \geq \dots \geq \text{Re } \lambda_{N-1}$, $\mathbf{y}(t)$ eventually converges to a periodic solution satisfying $\mathbf{y}(t) \propto \mathbf{v}_0(t)$ after a transient. Since $\mathbf{v}_0(t)$ should satisfy the normalization condition $\langle \mathbf{v}_0(t), \mathbf{u}_0(t) \rangle = 1$, we normalize $\mathbf{y}(t)$ at intervals of T as

$$\mathbf{y}(t) \rightarrow \frac{\mathbf{y}(t)}{\langle \mathbf{y}(t), \mathbf{u}_0(t) \rangle} \quad (\text{B3})$$

during the calculation.

2. Eigenvalues and eigenvectors for $i \geq 1$ (real)

We assume that the the eigenvalue and the eigenvectors $\{\lambda_i, \mathbf{u}_i(t), \mathbf{v}_i(t)\}$ ($i \geq 1$) are real and simple, and the eigenvalues and eigenvectors for $j = 0, 1, \dots, i - 1$ are already obtained.

We numerically integrate the linearized equation

$$\frac{d}{dt}\mathbf{y}(t) = \mathbf{J}(\mathbf{X}_0(t))\mathbf{y}(t) \quad (\text{B4})$$

from an arbitrary initial condition. During the calculation, we remove unnecessary vector components for $j = 0, 1, \dots, i-1$ to obtain the correct i th vector components (the vector components for $j = i+1, \dots, N-1$ have larger decay rates and automatically vanish). Namely, we subtract $\mathbf{u}_j(t)$ ($j = 0, 1, \dots, i-1$) at each time step as

$$\mathbf{y}(t) \rightarrow \mathbf{y}(t) - \sum_{j=0}^{i-1} \langle \mathbf{v}_j(t), \mathbf{y}(t) \rangle \mathbf{u}_j(t). \quad (\text{B5})$$

Since $\text{Re } \lambda_i > \text{Re } \lambda_{i+1} \geq \dots \geq \text{Re } \lambda_{N-1}$, the solution converges to $\mathbf{y}(t) \propto \mathbf{u}_i(t)$ after a transient. We assume the length of $\mathbf{u}_i(t)$ to be $|\mathbf{u}_i(t)| = 1$ (this can be arbitrary chosen and determines the scale of i th amplitude r_i) and normalize $\mathbf{y}(t)$ to satisfy $\langle \mathbf{y}(t), \mathbf{y}(t) \rangle = 1$ at each time step. After the transient, we take $\mathbf{y}(t)$ as a new initial state $\mathbf{y}(0)$ and calculate the eigenvalue λ_i as the growth rate of \mathbf{y} during one period of oscillation as

$$\lambda_i = \frac{1}{T} \ln \frac{\mathbf{y}(T)}{\mathbf{y}(0)}. \quad (\text{B6})$$

The right eigenvector $\mathbf{u}_i(t)$ can then be calculated by integrating

$$\frac{d}{dt}\mathbf{y}(t) = [\mathbf{J}(\mathbf{X}_0(t)) - \lambda_i]\mathbf{y}(t) \quad (\text{B7})$$

from $\mathbf{y}(0)$ for one period, which gives $\mathbf{u}_i(t) = \mathbf{y}(t)$ ($0 \leq t < T$).

We next calculate the left eigenvector $\mathbf{v}_i(t)$. We integrate the following equation from an arbitrary final condition backward in time:

$$\frac{d}{dt}\mathbf{y}(t) = -\mathbf{J}(\mathbf{X}_0(t))^\dagger \mathbf{y}(t). \quad (\text{B8})$$

During the calculation, we subtract the vector components in the directions $\mathbf{v}_j(t)$ ($j = 0, 1, \dots, j-1$) at each time step as

$$\mathbf{y}(t) \rightarrow \mathbf{y}(t) - \sum_{j=0}^{i-1} \langle \mathbf{y}(t), \mathbf{u}_j(t) \rangle \mathbf{v}_j(t). \quad (\text{B9})$$

Since $\text{Re } \lambda_i > \text{Re } \lambda_{i+1} \geq \dots \geq \text{Re } \lambda_{N-1}$, we eventually obtain $\mathbf{y}(t) \propto \mathbf{v}_i(t)$ after the transient. In order to satisfy the normalization condition $\langle \mathbf{v}_i(t), \mathbf{u}_i(t) \rangle = 1$, we periodically normalize $\mathbf{y}(t)$ at intervals of T as follows:

$$\mathbf{y}(t) \rightarrow \frac{\mathbf{y}(t)}{\langle \mathbf{y}(t), \mathbf{u}_i(t) \rangle}. \quad (\text{B10})$$

By using $\mathbf{y}(t)$ sufficiently after the initial transient as a new final state $\mathbf{y}(T)$, the left eigenvector can be calculated by backward integration of

$$\frac{d\mathbf{y}(t)}{dt} = -[\mathbf{J}(\mathbf{X}_0(t))^\dagger - \lambda_i^*]\mathbf{y}(t) \quad (\text{B11})$$

for one period ($0 \leq t < T$) as $\mathbf{v}_i(t) = \mathbf{y}(t)$.

3. Eigenvalues and eigenvectors for $i \geq 1$ (complex)

We assume that $\{\lambda_i, \mathbf{u}_i, \mathbf{v}_i\}$ and $\{\lambda_{i+1}, \mathbf{u}_{i+1}, \mathbf{v}_{i+1}\}$ for some $i \geq 1$ are mutually complex conjugate, namely, $\lambda_{i+1} = \lambda_i^*$, $\mathbf{v}_{i+1} = \mathbf{v}_i^*$, and $\mathbf{u}_{i+1} = \mathbf{u}_i^*$, and also $\text{Re } \lambda_i, \lambda_{i+1} > \text{Re } \lambda_{i+2}$. We also assume that the eigenvalues and eigenvectors for $j = 0, 1, \dots, i-1$ are already obtained. In this case, we cannot use the numerical method for the real vectors, so we calculate the complex eigenvalues and eigenvectors directly from the monodromy matrix $\mathbf{M} = \exp(\mathbf{\Lambda}T)$, denoted as $\mathbf{M} = [\mathbf{m}_0, \mathbf{m}_1, \dots, \mathbf{m}_{N-1}]$ where $\{\mathbf{m}_k \in \mathbb{R}^N\}_{k=0, \dots, N-1}$ are column vectors. By solving

$$\frac{d}{dt}\mathbf{y}(t) = \mathbf{J}(\mathbf{X}_0(t))\mathbf{y}(t) \quad (\text{B12})$$

from an arbitrary initial condition $\mathbf{y}(0)$ at $t = 0$ for one oscillation period T , we obtain $\mathbf{y}(T) = \exp(\mathbf{\Lambda}T)\mathbf{y}(0)$. By choosing a unit vector in the k th direction ($k = 0, \dots, N-1$) as the initial condition, i.e., $\mathbf{y}(0) = \mathbf{e}_k$, we can obtain $\mathbf{y}(T) = \mathbf{m}_i$ ($i = 0, \dots, N-1$). From the numerically evaluated \mathbf{M} and \mathbf{M}^\dagger , we can evaluate $\{\lambda_i, \mathbf{u}_i, \mathbf{v}_i\}$ and $\{\lambda_{i+1}, \mathbf{u}_{i+1}, \mathbf{v}_{i+1}\}$, i.e., the Floquet exponents and the Floquet eigenvectors at $\mathbf{X}_0(0)$.

The right eigenvectors $\mathbf{u}_{i'}(t)$ ($i' = i, i+1$) for $0 \leq t < T$ can be obtained by integrating

$$\frac{d}{dt}\mathbf{y}(t) = [\mathbf{J}(\mathbf{X}_0(t)) - \lambda_{i'}]\mathbf{y}(t) \quad (\text{B13})$$

from the initial condition $\mathbf{y}(0) = \mathbf{u}_{i'}$ ($i' = i, i+1$) for one oscillation period T . During the calculation, we subtract the components in the directions $\mathbf{u}_j(t)$ ($j = 0, 1, \dots, i-1$) at each time step as

$$\mathbf{y}(t) \rightarrow \mathbf{y}(t) - \sum_{j=0}^{i-1} \langle \mathbf{v}_j(t), \mathbf{y}(t) \rangle \mathbf{u}_j(t). \quad (\text{B14})$$

Next, the left eigenvectors $\mathbf{v}_{i'}(t)$ ($i' = i, i+1$) for $0 \leq t < T$ can be calculated by integrating

$$\frac{d}{dt}\mathbf{y}(t) = -[\mathbf{J}(\mathbf{X}_0(t))^\dagger - \lambda_{i'}^*]\mathbf{y}(t). \quad (\text{B15})$$

backward from the final condition $\mathbf{y}(T) = \mathbf{v}_{i'}$ ($i' = i, i + 1$). During the calculation, we subtract the coefficients in the directions of $\mathbf{v}_j(t)$ ($j = 0, 1, \dots, i - 1$) at each time step by

$$\mathbf{y}(t) \rightarrow \mathbf{y}(t) - \sum_{j=0}^{i-1} \langle \mathbf{y}(t), \mathbf{u}_j(t) \rangle \mathbf{v}_j(t). \quad (\text{B16})$$

In this method, we need to obtain an accurate monodromy matrix \mathbf{M} by using sufficiently small time steps for numerical integration. Also, it is not guaranteed in this method that the vector components in the directions of $\mathbf{u}_i(t)$ and $\mathbf{u}_{i+1}(t)$ and those in the directions of $\mathbf{v}_i(t)$ and $\mathbf{v}_{i+1}(t)$ do not mix due to numerical errors. The validity of the numerical results can be confirmed by checking the bi-orthonormality relation $\langle \mathbf{v}_j(t), \mathbf{u}_k(t) \rangle = \delta_{jk}$ for $j, k = i, i + 1$ after the calculation. If the numerical errors are non-negligible, we may need to introduce an additional bi-orthonormalization procedure to separate the vector components from each other. For the two examples used in this study, these numerical errors were negligible in our calculations. We also note that the method in this subsection can also be used to calculate real eigenvalues and eigenvectors, but the method in the previous subsection is numerically more accurate.

REFERENCES

- ¹James Pantaleone. Synchronization of metronomes. *American Journal of Physics*, 70(10):992–1000, 2002.
- ²Arthur T Winfree. Spiral waves of chemical activity. *Science*, 175(4022):634–636, 1972.
- ³John Buck and Elisabeth Buck. Mechanism of rhythmic synchronous flashing of fireflies: Fireflies of southeast asia may use anticipatory time-measuring in synchronizing their flashing. *Science*, 159(3821):1319–1327, 1968.
- ⁴John Buck and Elisabeth Buck. Synchronous fireflies. *Scientific American*, 234(5):74–85, 1976.
- ⁵G Bard Ermentrout and John Rinzel. Beyond a pacemaker’s entrainment limit: phase walk-through. *American Journal of Physiology-Regulatory, Integrative and Comparative Physiology*, 246(1):R102–R106, 1984.
- ⁶Albert Goldbeter. A model for circadian oscillations in the drosophila period protein (per). *Proceedings of the Royal Society of London. Series B: Biological Sciences*, 261(1362):319–324, 1995.

- ⁷Jean-Christophe Leloup, Didier Gonze, and Albert Goldbeter. Limit cycle models for circadian rhythms based on transcriptional regulation in drosophila and neurospora. *Journal of biological rhythms*, 14(6):433–448, 1999.
- ⁸Arthur T Winfree. *The geometry of biological time*. Springer, New York, 2001.
- ⁹Yoshiki Kuramoto. *Chemical oscillations, waves, and turbulence*. Springer, Berlin, 1984.
- ¹⁰G Bard Ermentrout and David H Terman. *Mathematical foundations of neuroscience*. Springer, New York, 2010.
- ¹¹Arkady Pikovsky, Michael Rosenblum, and Jürgen Kurths. *Synchronization: a universal concept in nonlinear sciences*. Cambridge University Press, Cambridge, 2001.
- ¹²Leon Glass and Michael C Mackey. *From clocks to chaos: the rhythms of life*. Princeton University Press, Princeton, 1988.
- ¹³SH Strogatz. *Nonlinear dynamics and chaos*. Westview Press, 1994.
- ¹⁴Kenichi Kawasaki, Yoshiyuki Akiyama, Kenji Komori, Masahiro Uno, Hidenori Takeuchi, Tomoari Itagaki, Yasufumi Hino, Yoshinobu Kawasaki, Katsuhisa Ito, and Ali Hajimiri. A millimeter-wave intra-connect solution. *IEEE Journal of Solid-State Circuits*, 45(12):2655–2666, 2010.
- ¹⁵Afshin S Daryoush. Optical synchronization of millimeter-wave oscillators for distributed architecture. *IEEE Transactions on microwave theory and techniques*, 38(5):467–476, 1990.
- ¹⁶Tomoharu Nagashima, Xiuqin Wei, Hisa-Aki Tanaka, and Hiroo Sekiya. Locking range derivations for injection-locked class-e oscillator applying phase reduction theory. *IEEE Transactions on Circuits and Systems I: Regular Papers*, 61(10):2904–2911, 2014.
- ¹⁷Dan Wilson and Jeff Moehlis. Spatiotemporal control to eliminate cardiac alternans using isostable reduction. *Physica D: Nonlinear Phenomena*, 342:32–44, 2017.
- ¹⁸Bharat Monga and Jeff Moehlis. Optimal phase control of biological oscillators using augmented phase reduction. *Biological cybernetics*, 113(1-2):161–178, 2019.
- ¹⁹Julia E Stone, Xavier L Aubert, Henning Maass, Andrew JK Phillips, Michelle Magee, Mark E Howard, Steven W Lockley, Shantha MW Rajaratnam, and Tracey L Sletten. Application of a limit-cycle oscillator model for prediction of circadian phase in rotating night shift workers. *Scientific reports*, 9(1):1–12, 2019.
- ²⁰Hiroya Nakao. Phase reduction approach to synchronisation of nonlinear oscillators. *Contemporary Physics*, 57(2):188–214, 2016.
- ²¹Bharat Monga, Dan Wilson, Tim Matchen, and Jeff Moehlis. Phase reduction and phase-

- based optimal control for biological systems: a tutorial. *Biological cybernetics*, 113(1-2):11–46, 2019.
- ²²Yoshiki Kuramoto and Hiroya Nakao. On the concept of dynamical reduction: the case of coupled oscillators. *Philosophical Transactions of the Royal Society A*, 377(2160):20190041, 2019.
- ²³Juan A Acebrón, Luis L Bonilla, Conrad J Pérez Vicente, Félix Ritort, and Renato Spigler. The kuramoto model: A simple paradigm for synchronization phenomena. *Reviews of modern physics*, 77(1):137, 2005.
- ²⁴Steven H Strogatz. From kuramoto to crawford: exploring the onset of synchronization in populations of coupled oscillators. *Physica D: Nonlinear Phenomena*, 143(1-4):1–20, 2000.
- ²⁵Sho Shirasaka, Wataru Kurebayashi, and Hiroya Nakao. Phase reduction theory for hybrid nonlinear oscillators. *Physical Review E*, 95(1):012212, 2017.
- ²⁶Kiyoshi Kotani, Ikuhiro Yamaguchi, Yutaro Ogawa, Yasuhiko Jimbo, Hiroya Nakao, and G Bard Ermentrout. Adjoint method provides phase response functions for delay-induced oscillations. *Physical Review Letters*, 109(4):044101, 2012.
- ²⁷Yoji Kawamura and Hiroya Nakao. Collective phase description of oscillatory convection. *Chaos: An Interdisciplinary Journal of Nonlinear Science*, 23(4):043129, 2013.
- ²⁸Hiroya Nakao, Tatsuo Yanagita, and Yoji Kawamura. Phase-reduction approach to synchronization of spatiotemporal rhythms in reaction-diffusion systems. *Physical Review X*, 4(2):021032, 2014.
- ²⁹Yuzuru Kato, Naoki Yamamoto, and Hiroya Nakao. Semiclassical phase reduction theory for quantum synchronization. *Phys. Rev. Research*, 1:033012, Oct 2019.
- ³⁰Jeff Moehlis, Eric Shea-Brown, and Herschel Rabitz. Optimal inputs for phase models of spiking neurons. *Journal of Computational and Nonlinear Dynamics*, 1(4):358–367, 2006.
- ³¹Isuru Dasanayake and Jr-Shin Li. Optimal design of minimum-power stimuli for phase models of neuron oscillators. *Physical Review E*, 83(6):061916, 2011.
- ³²Anatoly Zlotnik and Jr-Shin Li. Optimal entrainment of neural oscillator ensembles. *Journal of Neural Engineering*, 9(4):046015, 2012.
- ³³Jr-Shin Li, Isuru Dasanayake, and Justin Ruths. Control and synchronization of neuron ensembles. *IEEE Transactions on automatic control*, 58(8):1919–1930, 2013.
- ³⁴Takahiro Harada, Hisa-Aki Tanaka, Michael J Hankins, and István Z Kiss. Optimal waveform for the entrainment of a weakly forced oscillator. *Physical Review Letters*,

- 105(8):088301, 2010.
- ³⁵Hisa-Aki Tanaka. Optimal entrainment with smooth, pulse, and square signals in weakly forced nonlinear oscillators. *Physica D: Nonlinear Phenomena*, 288:1–22, 2014.
- ³⁶Hisa-Aki Tanaka, Isao Nishikawa, Jürgen Kurths, Yifei Chen, and István Z Kiss. Optimal synchronization of oscillatory chemical reactions with complex pulse, square, and smooth waveforms signals maximizes tsallis entropy. *EPL (Europhysics Letters)*, 111(5):50007, 2015.
- ³⁷Anatoly Zlotnik, Yifei Chen, István Z Kiss, Hisa-Aki Tanaka, and Jr-Shin Li. Optimal waveform for fast entrainment of weakly forced nonlinear oscillators. *Physical Review Letters*, 111(2):024102, 2013.
- ³⁸Sho Shirasaka, Nobuhiro Watanabe, Yoji Kawamura, and Hiroya Nakao. Optimizing stability of mutual synchronization between a pair of limit-cycle oscillators with weak cross coupling. *Physical Review E*, 96(1):012223, 2017.
- ³⁹Nobuhiro Watanabe, Yuzuru Kato, Sho Shirasaka, and Hiroya Nakao. Optimization of linear and nonlinear interaction schemes for stable synchronization of weakly coupled limit-cycle oscillators. *Physical Review E*, 100:042205, Oct 2019.
- ⁴⁰Arkady Pikovsky. Maximizing coherence of oscillations by external locking. *Physical Review Letters*, 115(7):070602, 2015.
- ⁴¹Anatoly Zlotnik, Raphael Nagao, István Z Kiss, and Jr-Shin Li. Phase-selective entrainment of nonlinear oscillator ensembles. *Nature Communications*, 7:10788, 2016.
- ⁴²Bharat Monga, Gary Froyland, and Jeff Moehlis. Synchronizing and desynchronizing neural populations through phase distribution control. In *2018 Annual American Control Conference (ACC)*, pages 2808–2813. IEEE, 2018.
- ⁴³Karsten Kuritz, Shen Zeng, and Frank Allgöwer. Ensemble controllability of cellular oscillators. *IEEE Control Systems Letters*, 3(2):296–301, 2019.
- ⁴⁴Bharat Monga and Jeff Moehlis. Phase distribution control of a population of oscillators. *Physica D: Nonlinear Phenomena*, 398:115–129, 2019.
- ⁴⁵Yuzuru Kato, Anatoly Zlotnik, Jr-Shin Li, and Hiroya Nakao. Optimization of periodic input waveforms for global entrainment of weakly forced limit-cycle oscillators. *arXiv preprint arXiv:2103.02880*, 2021.
- ⁴⁶Yoji Kawamura, Sho Shirasaka, Tatsuo Yanagita, and Hiroya Nakao. Optimizing mutual synchronization of rhythmic spatiotemporal patterns in reaction-diffusion systems.

- Physical Review E*, 96(1):012224, 2017.
- ⁴⁷Hiroya Nakao, Katunori Yamaguchi, Shingo Katayama, and Tatsuo Yanagita. Sparse optimization of mutual synchronization in collectively-oscillating networks. *in preparation*, 2021.
- ⁴⁸Yuzuru Kato and Hiroya Nakao. Semiclassical optimization of entrainment stability and phase coherence in weakly forced quantum limit-cycle oscillators. *Physical Review E*, 101(1):012210, 2020.
- ⁴⁹Igor Mezić. Spectral properties of dynamical systems, model reduction and decompositions. *Nonlinear Dynamics*, 41(1-3):309–325, 2005.
- ⁵⁰Igor Mezić. Analysis of fluid flows via spectral properties of the koopman operator. *Annual Review of Fluid Mechanics*, 45:357–378, 2013.
- ⁵¹Alexandre Mauroy, Igor Mezić, and Jeff Moehlis. Isostables, isochrons, and koopman spectrum for the action–angle representation of stable fixed point dynamics. *Physica D: Nonlinear Phenomena*, 261:19–30, 2013.
- ⁵²Dan Wilson and Jeff Moehlis. Isostable reduction of periodic orbits. *Physical Review E*, 94(5):052213, 2016.
- ⁵³Alexandre Mauroy and Igor Mezić. Global computation of phase-amplitude reduction for limit-cycle dynamics. *Chaos: An Interdisciplinary Journal of Nonlinear Science*, 28(7):073108, 2018.
- ⁵⁴Sho Shirasaka, Wataru Kurebayashi, and Hiroya Nakao. Phase-amplitude reduction of transient dynamics far from attractors for limit-cycling systems. *Chaos*, 27(2):023119, 2017.
- ⁵⁵Sho Shirasaka, Wataru Kurebayashi, and Hiroya Nakao. Phase-amplitude reduction of limit cycling systems. In *The Koopman Operator in Systems and Control*, pages 383–417. Springer, 2020.
- ⁵⁶Kiyoshi Kotani, Yutaro Ogawa, Sho Shirasaka, Akihiko Akao, Yasuhiko Jimbo, and Hiroya Nakao. Nonlinear phase-amplitude reduction of delay-induced oscillations. *Physical Review Research*, 2(3):033106, 2020.
- ⁵⁷Hiroya Nakao. Phase and amplitude description of complex oscillatory patterns in reaction-diffusion systems. In *Physics of Biological Oscillations*. Springer, to be published, 2021.
- ⁵⁸Dan Wilson and Bard Ermentrout. Greater accuracy and broadened applicability of phase reduction using isostable coordinates. *Journal of mathematical biology*, 76(1):37–66, 2018.

- ⁵⁹Dan Wilson. Optimal control of oscillation timing and entrainment using large magnitude inputs: An adaptive phase-amplitude-coordinate-based approach. *arXiv preprint arXiv:2102.04535*, 2021.
- ⁶⁰Bard Ermentrout. Type i membranes, phase resetting curves, and synchrony. *Neural computation*, 8(5):979–1001, 1996.
- ⁶¹Eric Brown, Jeff Moehlis, and Philip Holmes. On the phase reduction and response dynamics of neural oscillator populations. *Neural computation*, 16(4):673–715, 2004.
- ⁶²Dominic William Jordan and Peter Smith. *Nonlinear ordinary differential equations: an introduction to dynamical systems*, volume 2. Oxford University Press, USA, 1999.
- ⁶³John Guckenheimer and Philip Holmes. *Nonlinear oscillations, dynamical systems, and bifurcations of vector fields*, volume 42. Springer Science & Business Media, 2013.
- ⁶⁴Frank C Hoppensteadt and Eugene M Izhikevich. *Weakly Connected Neural Networks*, volume 126. Springer, 1997.
- ⁶⁵Balth Van der Pol and Jan Van Der Mark. Frequency demultiplication. *Nature*, 120(3019):363–364, 1927.
- ⁶⁶Balth Van der Pol. Vii. forced oscillations in a circuit with non-linear resistance.(reception with reactive triode). *The London, Edinburgh, and Dublin Philosophical Magazine and Journal of Science*, 3(13):65–80, 1927.
- ⁶⁷K-D Willamowski and OE Rössler. Irregular oscillations in a realistic abstract quadratic mass action system. *Zeitschrift für Naturforschung A*, 35(3):317–318, 1980.
- ⁶⁸Richard P Boland, Tobias Galla, and Alan J McKane. Limit cycles, complex floquet multipliers, and intrinsic noise. *Physical Review E*, 79(5):051131, 2009.
- ⁶⁹Pascale Geysermans and Florence Baras. Particle simulation of chemical chaos. *The Journal of chemical physics*, 105(4):1402–1408, 1996.
- ⁷⁰Baltazar D Aguda and Bruce L Clarke. Dynamic elements of chaos in the willamowski-rössler network. *The Journal of chemical physics*, 89(12):7428–7434, 1988.